Jong Min Lee[1]
Ji-eun Kim[1]
Jayant Borana[2]
Bong Hyun Chung[3]
Bong Geun Chung[4]

[1]Department of Bionano Technology, Hanyang University, Ansan, Korea
[2]Department of Chemical Engineering, Indian Institute of Technology, Guwahati, India
[3]BioNanotechnology Research Center, Korea Research Institute of Bioscience and Biotechnology, Daejeon, Korea
[4]Department of Mechanical Engineering, Sogang University, Seoul, Korea

Received October 23, 2012
Revised January 29, 2013
Accepted February 27, 2013

Research Article

Dual-micropillar-based microfluidic platform for single embryonic stem cell-derived neuronal differentiation

We developed the dual-micropillar-based microfluidic platform to direct embryonic stem (ES) cell fate. 4 × 4 dual-micropillar-based microfluidic platform consisted of 16 circular-shaped outer micropillars and 8 saddle-shaped inner micropillars in which single ES cells were cultured. We hypothesized that dual-micropillar arrays would play an important role in controlling the shear stress and cell docking. Circular-shaped outer micropillars minimized the shear stress, whereas saddle-shaped inner micropillars allowed for docking of individual ES cells. We observed the effect of saddle-shaped inner micropillars on cell docking in response to hydrodynamic resistance. We also demonstrated that ES cells cultured for 6 days within the dual-micropillar-based microfluidic platform differentiated into neural-like cells. Therefore, this dual-micropillar-based microfluidic platform could be a potentially powerful method for screening of lineage commitments of single ES cells.

Keywords:
Embryonic stem cell / Microfluidic device / Neuronal differentiation
DOI 10.1002/elps.201200578

Additional supporting information may be found in the online version of this article at the publisher's web-site

1 Introduction

Embryonic stem (ES) cells are powerful cell types to regulate lineage commitment in cell-based replacement therapies. In particular, ES cell-derived neuronal differentiation has previously been investigated for potential applications in neuronal tissue repairs and neurodegenerative diseases [1, 2]. For instance, treatment of rat ES cells with retinoic acid induced neuronal and glial differentiation [3]. It demonstrated the effect of retinoic acid on neuronal and glial differentiation, showing that the neuronal expression was increased up to 70% after 14 days of retinoic acid treatment, whereas glial cells were highly expressed after 10 days. The differentiation of rat ES cells into endothelial cells was markedly induced by Matrigel substrates, resulting in forming vascular tube-like network structures. The electrophysiological properties of ES cell-derived neurons have been investigated using a whole-cell patch-clamp recording system [4]. Tubulin-positive neuronal lineages were derived from embryoid bodies (EBs) and analysis of the spontaneous synaptic currents showed that the synaptic activity was enhanced by glutamate treatment. Western blot analysis demonstrated that synaptophysin was highly expressed in mouse ES cell-derived neurons. Furthermore, cerebral cortical projection neurons have been differentiated from human ES cells and induced pluripotent stem cells [5]. It was observed that induced pluripotent stem cells differentiated into glutamatergic projection neurons. A cortical slice culture assay also showed that human-induced pluripotent stem cell-derived neurons were radially oriented in the mouse cortex and their neurites were directed between the pial and ventricular surfaces.

Various microengineering platforms (e.g., microwell arrays, microfluidic devices) have previously been developed to direct ES cell fate. Polymeric microwell arrays are of great benefit for directing ES cell-derived specific lineage differentiation. For example, poly(ethylene glycol) (PEG) hydrogel microwell arrays have been used to culture uniform-sized ES cells [6, 7]. Engineered PEG microwell arrays enabled the control of uniform-sized EBs [6], indicating that lineage-specific differentiation was regulated by EB sizes. Cardiogenesis and vasculogenesis was significantly affected by uniform sizes (e.g., 150, 300, and 450 μm in diameter) of EBs, indicating that cardiogenesis was markedly induced in larger PEG microwells, while endothelial cell differentiation was decreased

Correspondence: Professor Bong Geun Chung, Department of Mechanical Engineering, Sogang University, Seoul, Korea
E-mail: bchung@sogang.ac.kr

Abbreviations: **EB**, embryoid body; **ES**, embryonic stem; **ITS**, insulin-transferrin-selenium; **Tuj1**, β-tubulin

Colour Online: See the article online to view Fig. 1–4 in colour.

with increasing EB sizes [7]. The Wnt signaling pathway was found to enable control of the fate of EB-derived vasculogenesis and cardiogenesis, showing that Wnt 5a and Wnt 11 were highly expressed in smaller and larger EBs, respectively. Polyurethane-based microwell arrays have been generated to control the cardiogenesis of human ES cells [8]. E-cadherin was highly expressed and β–catenin was co-localized in deeper microwells, suggesting that cell–cell interactions were enhanced in polyurethane microwells compared to adherent cells. It was revealed that canonical Wnt activation enabled the control of the fate of ES cell differentiation, indicating that Wnt signaling of EBs cultured within the microwells was upregulated to induce cardiogenesis. Poly(dimethylsiloxane) (PDMS)-based concave microwell arrays have also been used to regulate neuronal differentiation from murine ES cells [9]. EB sizes were significantly affected by the width (e.g., 200, 500, and 1000 μm) of the microwells, showing that uniformly sized EBs were created within concave microwell arrays. These findings demonstrated the effect of uniformly sized EBs on neuronal differentiation, indicating that ES cells cultured within larger concave microwells (500, 1000 μm in width) were more differentiated into neural-like cells. The neurite outgrowth activity was higher in larger microwells compared to smaller microwells (200 μm in width).

Microfluidic devices have been used to understand the cell biology [10–14]. In particular, single cell-based microfluidic culture platforms have recently been developed [15–17]. For instance, 10 × 10 microfluidc array has been used to regulate cell growth kinetic, passage cycle, and real-time analysis [15]. This microfluidic device consisted of circular-shaped microchambers, concentration gradient generators, and multiple perfusion microchannels that could continuously provide culture medium to main microchambers. The human carcinoma (HeLa) cell suspension and medium was applied into microchambers in a sequential manner. It demonstrated that the growth rate of HeLa cells was significantly affected by perfusion flow rates, showing the highest growth rate at 0.12 μL/min flow rate and double time of 1.4 days. The dynamic single cell culture array has been developed in the microfluidic device [16]. This platform containing U-shaped hydrodynamic branched trapping microarrays enabled the control of dynamic fluidic perfusion. Single HeLa cells were uniformly docked within U-shaped trapping arrays (10 μm in depth). The computational modeling analysis represented the effect of spherical U-shaped arrays on shear stress, indicating shear sheltering effect inside U-shaped hydrodynamic trapping microarrays. 90% individual HeLa cells trapped inside U-shaped trapping microarrays were adhered and were subsequently divided within 24 hours, while 5% cells became apoptotic. The single cell–cell interaction has been investigated in the microfluidic coculture device [17]. This platform consisted of semi-isolated C-shaped culture microchambers (400 μm in diameter) and gradient generators. Large number of heterotypic pairing on ES cells and embryonic fibroblast cells in C-shaped microchannels was observed, showing that the cells were preferentially docked at the trapping junctions (3 μm in width) due to self-variable fluidic resistance. These trapped cells were moved away from trapping junctions to form heterotypic pairs.

Recently, microfluidic culture devices have been developed to regulate stem cell-derived specific lineage differentiation [18–21]. Compartmentalized microfluidic devices have been used to regulate uniform EB sizes and their neuronal differentiation [18]. The cross-sectional size of microchannels and semi-porous polymeric membranes sandwiched in two-layer microchannels enabled the control of nonattached and uniform-sized EBs [18]. It was observed that the size of EBs grown in a compartmentalized microfluidic device increased with culture times and EBs were exposed to the culture medium through semi-porous membranes. Furthermore, uniformly sized EBs (50∼200 μm in diameter) harvested from microchannels differentiated into neural-like cell lineages. ES cell-derived neurons have also been cultured in the compartmental microfluidic devices [19]. EBs were shown to easily settle out through the holes in the main microchannels, and middle-stage (5∼7 days) EBs were used to induce EB-derived neuronal differentiation. Axons of mouse ES cell-derived neurons were isolated and traversed through bridge-shaped microgroove channels. The transportation of mitochondria, which could have the potential to deliver energy to cell bodies in ES cell-derived neurons, was tracked in a real-time manner. The effect of fluidic flow-induced shear stress on self-renewal of mouse ES cells has been investigated in the multiplex logarithmic microfluidic device [20]. The fluidic flow-induced shear stress played an important role in regulating the growth and phenotype of ES cell colony, indicating that the adhesion of ES cell colony was inversely proportional to the shear stress. The growth of ES cell colony was decreased by removing soluble factors. This study demonstrated that fluidic flow-induced shear stress increased the expression of epiblast marker (e.g., Fig 5) and the self-renewal of ES cells were mechanically affected by shear stress via heparin sulfate proteoglycans (HSPGs), which has been known to transduce fluidic flow-induced shear stress in endothelial cells. Furthermore, a two-layer microfluidic perfusion device containing pneumatically actuated microvalves has been used to regulate the diffusible signaling of mouse ES cells [21]. This study demonstrated the effect of the cell-secreted factors (e.g., autocrine, paracrine) on self-renewal and neuroectoderm specification, showing that the fluidic flow inhibited the autocrine loop of fibroblast growth factor 4 (FGF4) that could play an important role in inducing neuroectoderm differentiation. This study revealed that the proliferation and neuroectoderm differentiation of mouse ES cells was suppressed by removing cell-secreted factors. However, previous approaches did not consider the effect of shear-sheltering dual-micropillar arrays on uniform docking of single ES cells and neuronal differentiation in the microfluidic device. In this paper, we developed the dual-micropillar-based microfluidic device containing circular-shaped outer micropillars and saddle-shaped inner micropillars. Individual ES cells were docked within shear-sheltered dual-micropillars and the hydrodynamic resistance enabled the control of docking of single ES cells. We also demonstrated that single ES cells cultured for 6 days in

dual-micropillar-based microfluidic device differentiated into neural-like cells.

2 Materials and methods

2.1 Fabrication of the dual-micropillar-based microfluidic platform and experimental setup

The 4 × 4 dual-micropillar-based microfluidic platform consisted of 16 circular-shaped outer micropillars and 8 saddle-shaped inner micropillars. We developed circular-shaped outer micropillars (36 μm in diameter) and saddle-shaped inner micropillars (60 μm in width, 36 μm in height) in the micropillar array (500 μm in diameter). To fabricate 4 × 4 dual-micropillar-based fluidic channel, hexamethyldisilazane (Sigma Aldrich, USA) was spin-coated onto a 3 inch silicon wafer (Buysemi Co., Korea) and AZ photoresist (AZP4620, AZ Electronic Materials, USA) was subsequently applied. The photoresist was then exposed to UV light (S1500A, Omnicure, Canada) for 30 s through a mask film. To generate round-shaped fluidic microchannels, the photoresist-patterned silicon wafer was post-baked at 130°C for 2 min. We also fabricated pneumatic control channels with 40 μm thickness using SU-8 photoresist (MicroChem, MA, USA), as previously described [22]. To fabricate the microvalves inside the dual-micropillar-based microfluidic platform, pneumatic control microchannels and 4 × 4 dual-micropillar-based fluidic channels were orthogonally aligned after oxygen plasma treatment (Femto Scientific, Korea) (Fig. 1A). After alignment, the dual-micropillar-based microfluidic platform was bonded to the glass substrate to culture single ES cells. Cell seeding and medium perfusion (0.03 μL/min flow rate, 5×10^{-4} m/s inlet velocity) were performed by actuating the microvalves in a sequential manner (Fig. 1B–D). ES cells were cultured for 6 days in the dual-micropillar-based microfluidic platform. Phase contrast and fluorescent images were taken using an inverted fluorescent microscope (Olympus IX71, Japan) and their images were analyzed by Image J program.

2.2 Computational simulation of the shear stress

Computational fluid dynamics model was used to predict shear stress as a function of the average inlet flow rate for different depths (d = 3 μm, 6 μm, 12 μm) using FEMLAB software (COMSOL 3.5). We performed modeling using different depth (d) of inner micropillar arrays (3 μm, 6 μm, 12 μm). The perfusion medium was modeled as an incompressible, homogeneous, Newtonian fluid with the same properties of water with a density (ρ) of 1000 kg/m^3 and a viscosity (η) of 0.001 Pa·s. The steady-state Navier-Stokes equations for incompressible newtonian fluids [23] were solved using COMSOL:

$$\nabla \cdot v = 0, \tag{1}$$

$$\rho v \cdot \nabla v = -\nabla p + \eta \nabla^2 v, \tag{2}$$

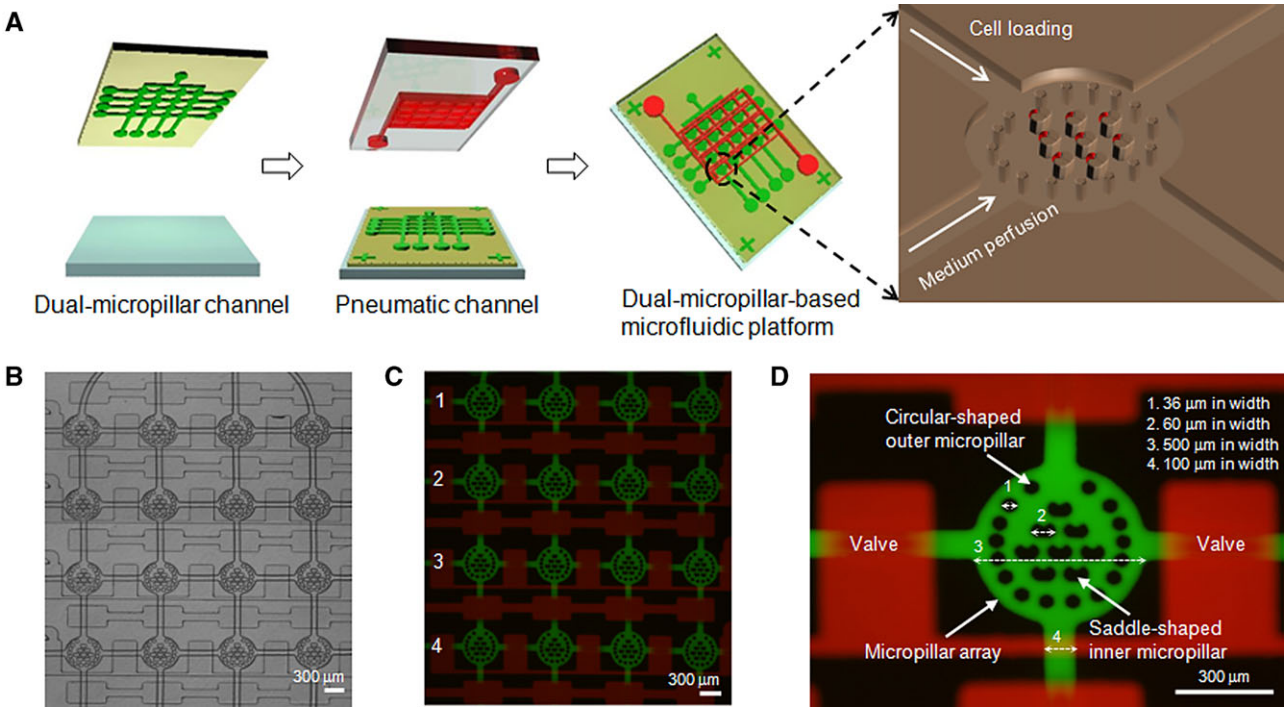

Figure 1. Dual-micropillar-based microfluidic platform. (A) Schematic of the fabrication process. (B) Phase contrast image of the 4 × 4 dual-micropillar-based microfluidic platform. (C and D) Fluorescent image of the dual-micropillar-based microfluidic platform containing microvalves.

where v and p are velocity vector and pressure. No-slip boundary conditions were applied for the channel and micropillar walls. Inlet velocities of 1.667×10^{-4} to 16.67×10^{-4} m/s were applied to simulate a flow rate ranging from 0.01 to 0.1 μL/min. A zero pressure condition was applied to outlet. The fluidic domain was meshed using finer mesh. The numbers of elements in entire mesh were 78 397, 79 791, and 85 029 in 3 μm, 6 μm, and 12 μm deep saddle-shaped inner micropillars, respectively.

2.3 ES cell culture

We cultured murine ES cells (R1 cell line) in a tissue culture dish containing 0.1% gelatin. ES cells were cultured with DMEM with 15% ES cell-qualified FBS (Invitrogen, CA, USA), 1400 units/mL leukemia inhibitory factor (Millipore, MA, USA), 1% nonessential amino acid solution, 0.1% beta-mercatoethanol, and 1% penicillin-streptomycin. To induce ES cell-derived neuronal differentiation, we used DMEM F12 (Invitrogen) with 0.16% D glucose, 1% insulin-transferrin-selenium (ITS) supplement, 1% N2 supplement, and 1% penicillin-streptomycin.

2.4 Immunocytochemistry

ES cells cultured for 6 days in the dual-micropillar-based microfluidic platform were fixed with 4% paraformaldehyde for 30 min at room temperature and were subsequently permeabilized with 1% Triton X-100 in PBS for 15 min. After washing, they were blocked with 1% BSA for 2 h at room temperature. ES cells were immunostained with the primary antibodies (anti-neuronal classIII, β-tubulin (Tuj1) (Stem Cell Technology, Canada), and anti-α-smooth muscle actin (SMA) (Abcam)) overnight and were subsequently incubated with secondary antibodies (Alexa Fluor 488 goat anti-mouse IgG and Alexa Fluor 594 chicken anti-rabbit IgG (Invitrogen)) for 3–4 h at room temperature.

3 Results and discussion

3.1 Fabrication of dual-micropillar-based microfluidic platform

We fabricated a microfluidic platform containing 4 × 4 dual-micropillar arrays to culture single ES cells (Fig. 1). Individual ES cells were seeded into dual-micropillar arrays through the top inlet microchannel and the medium was orthogonally perfused from the left inlet microchannel using pneumatically actuated microvalves in a sequential manner. The dual-micropillar array consisted of 16 outer micropillars and 8 saddle-shaped inner micropillars. We hypothesized that outer micropillars (12∼20 μm distance between micropillars) would minimize the shear stress and the saddle-shaped inner micropillars would allow for docking of individual ES cells. We have previously developed an integrated microfluidic culture platform containing single micropillar arrays to regulate ES cell-derived endothelial cell differentiation [22]. It demonstrated the effect of the intervals between single micropillars on the shear stress, showing that the shear stress was negligible inside micropillar arrays in which the distance of micropillars was narrow (12 μm). It was also observed that ES cells cultured in the integrated microfluidic culture platform were differentiated into endothelial cells. However, this previous approach did not consider the effect of dual-micropillars on the shear stress.

3.2 Computational simulation of the shear stress within dual-micropillars

To predict the velocity profile and shear stress within dual-micropillar arrays, we performed the computational fluidic dynamics using FEMLAB software (Fig. 2). To predict the velocity profile inside the dual-micropillar arrays, we employed the Navier-Stokes equations and 0.03 μL/min average inlet flow rate (Fig. 2A). Most streamlines of velocity profiles were shown between the outer and inner micropillars. In contrast, the streamline of velocity profiles generated from the top inlet microchannel did not penetrate into the center of the saddle-shaped inner micropillars due to the higher hydrodynamic resistance. As a result, we expect that streamline of velocity profiles would enable the control of cell docking inside the saddle-shaped inner micropillars in a spatial manner. We also simulated the shear stress induced by fluidic flows from the left inlet microchannel within the dual-micropillar arrays (Fig. 2B). To model the shear stress on the bottom surface of the X-axis in the dual-micropillars, we used 0.01∼0.1 μL/min average inlet flow rates. Computational modeling showed that the shear stress inside the saddle-shaped inner micropillars was negligible. The shear stress was higher at the place (e.g., inlet microchannel) where velocity was higher or was rapidly changed. The simulation of shear stress patterns was performed with respect to different depths (d = 3, 6, 12 μm, Fig. 2C) of saddle-shaped inner micropillars (Fig. 2D). The simulation analysis revealed that the shear stress linearly increased with inlet flow rates and it was highly negligible at the deep saddle-shaped inner micropillar (d = 12 μm). We also investigated the effect of total heights (e.g., 36, 42, and 48 μm) of saddle-shaped inner micropillars on shear stress profiles, showing no significant difference of the shear stress (data not shown). It demonstrated that shear stress profiles were largely affected by depths of saddle-shaped inner micropillars. From computational modeling results, we optimized the depth (12 μm) of the saddle-shaped inner micropillars to protect the cells from the shear stress. A microsieve-based microfluidic device has previously been fabricated for programmed trapping of individual bacteria [24]. Three different types (e.g., 0°, 15°, and 30° entry angle) of U-shaped microsieves were used to trap individual bacterial cells. It demonstrated the effect of the hydrodynamic resistance on trapping performance in microsieves, showing that movement of the cell docking decreased with increasing hydrodynamic resistance. It

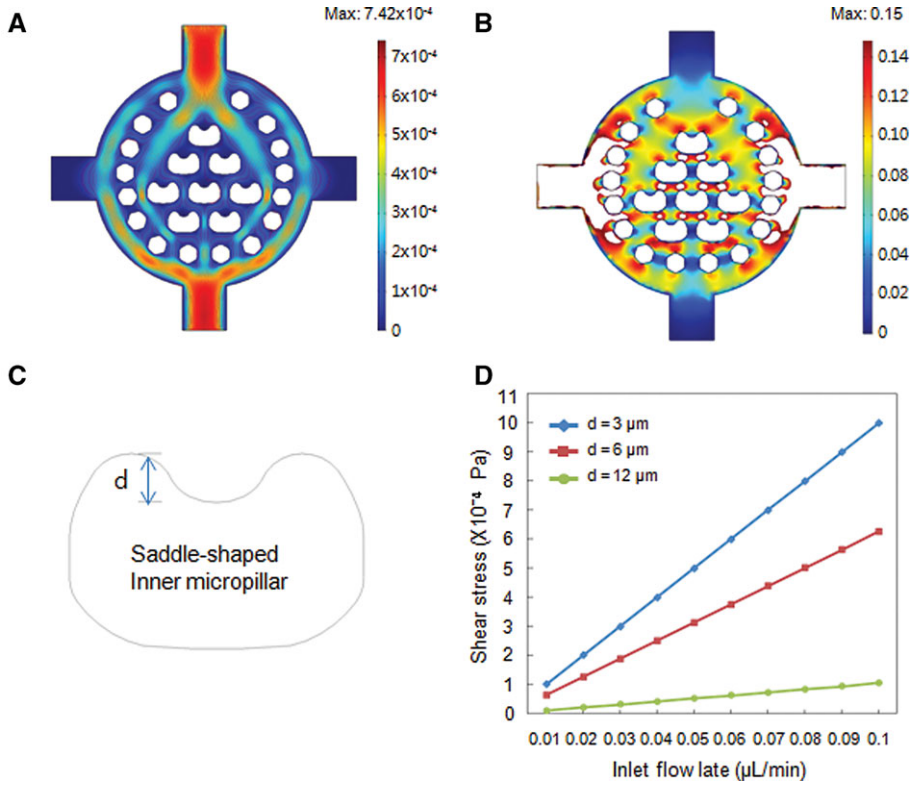

Figure 2. Analysis of the velocity profile and shear stress in the dual-micropillar-based microfluidic device. (A) Modeling of velocity profiles in the dual-micropillar-based microfluidic device (0.03 μL/min average inlet flow rate from the top microchannel). (B) Modeling of shear stress profile in response to the flow rate (0.03 μL/min average inlet flow rate from the left microchannel). (C) Schematic shape (d = depth) of the saddle-shaped inner micropillar. (D) Analysis of shear stress profiles in the saddle-shaped inner micropillar arrays containing different depths (d = 3, 6, 12 μm).

observed that the probability of the cell trapping was inversely proportional to the entry angles, indicating that the fraction of occupied microsieves was higher at a 0° entry angle. Despite its potential to trap the bacteria within microsieves, the previous approach did not consider the effect of U-shaped microsieve structures on docking of individual mammalian cells, such as stem cells.

3.3 Analysis of cell docking within dual-micropillars

We investigated cell docking within saddle-shaped inner micropillars after theoretical analysis of the velocity profile and shear stress within dual-micropillar arrays (Fig. 3). We observed that individual ES cells were trapped within the saddle-shaped inner micropillars (Fig. 3A). Although some cells were located around the outer micropillars, most individual ES cells were docked within the saddle-shaped inner micropillars. We analyzed the effect of the flow rate on the cell docking within saddle-shaped inner micropillars, indicating that the number of docked cells was proportional to the applied flow rate (Fig. 3B). The cells were preferentially docked in arrays 1∼2 compared to arrays 3∼4, when a 1 μL/min flow rate was applied to the microchannels. In contrast, we found that cells (3∼5 cells in each array) were uniformly occupied in arrays 1∼4, when a higher velocity (e.g., 5∼10 μL/min) was employed. Array 1, which contains four dual-micropillar arrays, is close to the top inlet microchannel (Fig. 1C). We also analyzed the effect of the spatial position (positions A∼H) of the saddle-shaped inner micropillars on cell docking in array 3 (Fig. 3C). Quantitative analysis showed the smallest number of cells docked at position E, because of the higher hydrodynamic resistances at position E (Fig. 2A). For the dual-micropillar-based microfluidic device, outer micropillars helped to generate the uniform velocity and shear stress. Thus, most of the fluid did not pass through the center of the microchannels. If we only use inner micropillars without outer micropillars, the cells would be directly exposed to shear stress and they could not be uniformly docked in all positions (positions A–H) of inner micropillars, because most of the fluid passes through center of the microfluidic device. Therefore, the outer micropillars could provide shear-sheltering effect of the ES cells and help to guide better docking of individual ES cells.

3.4 Single ES cell-derived neuronal differentiation

To investigate the feasibility of our microfluidic platform for the single ES cell-derived neuronal differentiation, ES cells were cultured for 6 days in the dual-micropillar-based microfluidic platform (Fig. 4). To induce the ES cell-derived neuronal differentiation, we employed ITS and N2 supplements. To compare the single ES cell-derived neuronal differentiation in the glass-based microfluidic device, we performed glass-based control experiments (Fig. 4A and B). We observed that single ES cells cultured with ITS and N2 supplements differentiated into Tuj1-positive neurons compared

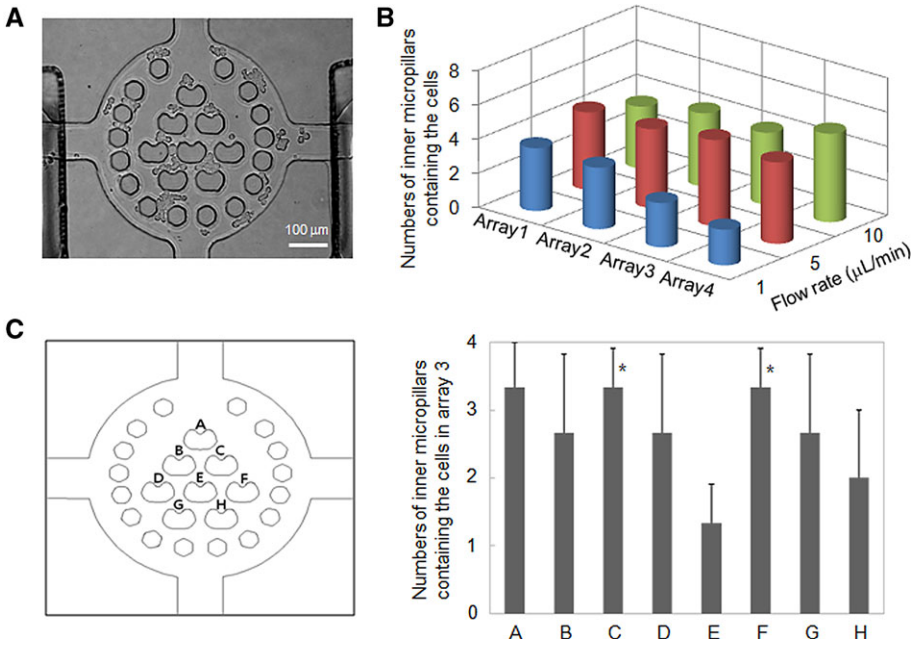

Figure 3. Analysis of ES cell docking in the dual-micropillar-based microfluidic platform. (A) Phase contrast image of single ES cell docking inside the saddle-shaped inner micropillars. (B) Quantitative analysis of cell docking inside the saddle-shaped inner micropillars. Arrays 1 and 4 of the dual-micropillar arrays are close to the cell seeding inlet and outlet, respectively. (C) Schematic of positions A∼H in the saddle-shaped inner micropillars and quantification of cell docking at positions A∼H of the saddle-shaped inner micropillars in array 3. 5 μL/min flow rate is used for the cell docking experiment and all data are compared to position E (*$p < 0.05$).

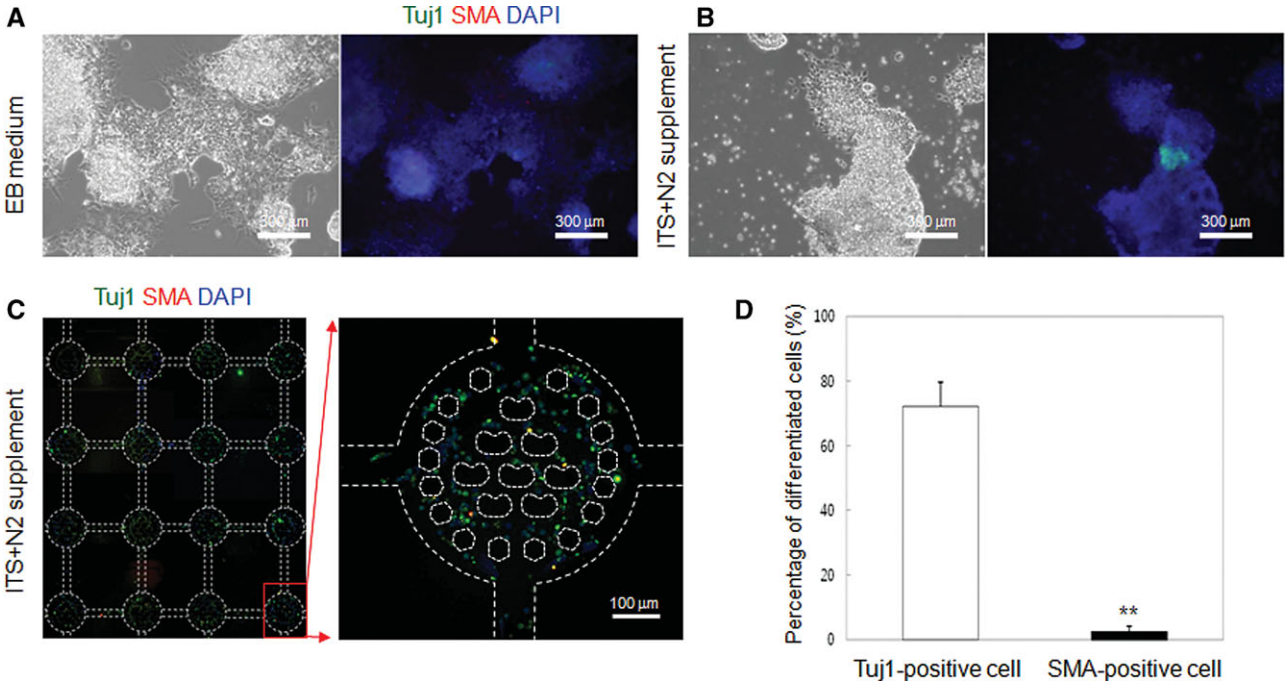

Figure 4. Single ES cell-derived neuronal differentiation in the dual-micropillar-based microfluidic platform. (A and B) Phase contrast and fluorescent images of ES cells cultured for 6 days with EB medium alone and ITS + N2 supplement on glass-based substrates. (C) Neural-like cells derived from single ES cells in the dual-micropillar-based microfluidic platform. Tuj1 and SMA are indicated by green and red colors, respectively. White dot lines represent dual-micropillar arrays in the microfluidic device. (D) Quantitative analysis of the single ES cell-derived neural-like cells in the dual-micropillar-based microfluidic platform (**$p < 0.01$).

to EB medium alone. Interestingly, ES cells cultured with EB medium alone were spread (Fig. 4A), whereas ES cells cultured with ITS and N2 supplements were not elongated (Fig. 4B). It was probably due to serum-free ITS supplements that could induce cell death except nestin-positive neural progenitor cells derived from ES cells, as previously described [25]. In parallel, ES cells were cultured for 6 days in the dual-micropillar-based microfluidic platform. Immunocytochemistry demonstrated that Tuj1-positive neural-like cells were markedly expressed in the

dual-micropillar-based microfluidic platform, showing that 72% single ES cells differentiated into neural-like cells (Fig. 4C and D). Similar to the glass-based control with ITS and N2 supplements (Fig. 4B), the morphology of single ES-cell-induced neural-like cells in the dual-micropillar-based microfluidic platform was round (Fig. 4C). It was probably due to continuous medium perfusion and glass-based substrate. To further confirm ES cell-derived neuronal differentiation, we also stained ES cells using different neural markers, such as neuronal nucleus marker and microtubule-associated protein2. It showed that the percentage of neuronal nucleus marker-positive cells and microtubule-associated protein2-positive cells was 74% and 68%, respectively (Supporting Information Fig. 1). A microfluidic device containing microwell arrays has previously developed to induce neuronal differentiation of mouse embryonic carcinoma cells [26]. The cells were seeded into microchannels and were subsequently docked within microwells, showing that the size (~150 μm in diameter) of EBs was manipulated by the flow rate and cell density. This result demonstrated that EBs cultured with retinoic acid in the absence of serum were more likely to differentiate into neural-like cells. A 3 × 3 multilayer microfluidic array device containing concave microwells has also been generated for uniformly sized EB-derived neuronal differentiation [27]. EBs were generated within concave microwells and were subsequently replated into flat cell culture chambers without manual cell retrieval in the microfluidic device. It was observed that uniform cell docking was controlled by flow rates and EB sizes were increased with increasing culture times, showing 450 μm in diameter on day 3. This study also demonstrated neuronal differentiation from mouse EBs, which were replated on flat cell culture chambers in the microfluidic device. Despite their potential to control EB-induced neuronal differentiation in the microfluidic devices, previous approaches mainly explored EB-derived neuronal differentiation. In this paper, we investigate the effect of dual-micropillar arrays on uniform docking of single ES cells and neuronal differentiation in the microfluidic device. Therefore, this dual-micropillar-based microfluidic platform is a powerful tool to control the single ES cell-derived neuronal differentiation.

4 Concluding remarks

We developed the dual-micropillar-based microfluidic platform to regulate single ES cell-derived neuronal differentiation; 4 × 4 dual-micropillar-based microfluidic platform consisted of 16 circular-shaped outer micropillars and 8 saddle-shaped inner micropillars. We demonstrated the effect of dual-micropillar arrays on uniform docking of single ES cells, showing that the probability of individual ES cell docking decreased at the center of the saddle-shaped inner micropillars due to higher hydrodynamic resistance. We also observed that the single ES cells cultured for 6 days within the dual-micropillar-based microfluidic platform differentiated into neural-like cells (72%). Therefore, this microfluidic platform could be a potentially powerful tool to regulate single ES cell-derived neuronal differentiation.

This paper was supported by the National Research Foundation of Korea (NRF) grant funded by the Ministry of Education, Science and Technology (Grant Number 20100004869, 20110016331, 2012R1A1A2005822). This research was supported by a grant from the Korea Research Institute of Bioscience and Biotechnology (KRIBB) Initiative Research Program (Grant number KGM7141111). This work was also supported by the Sogang University Research Grant of 2013.

The authors have declared no conflict of interest.

5 References

[1] Gaspard, N., Bouschet, T., Hourez, R., Dimidschstein, J., Naeije, G., van den Ameele, J., Espuny-Camacho, I., Herpoel, A., Passante, L., Schiffmann, S. N., Gaillard, A., Vanderhaeghen, P., *Nature* 2008, *455*, 351–357.

[2] Eiraku, M., Watanabe, K., Matsuo-Takasaki, M., Kawada, M., Yonemura, S., Matsumura, M., Wataya, T., Nishiyama, A., Muguruma, K., Sasai, Y., *Stem Cell* 2008, *3*, 519–532.

[3] Ruhnke, M., Ungefroren, H., Zehle, G., Bader, M., Kremer, B., Fandrich, F., *Stem Cell* 2003, *21*, 428–436.

[4] Bibel, M., Richter, J., Schrenk, K., Tucker, K. L., Staiger, V., Korte, M., Goetz, M., Barde, Y. A., *Nat. Neurosci.* 2004, *7*, 1003–1009.

[5] Shi, Y., Kirwan, P., Smith, J., Robinson, H. P., Livesey, F. J., *Nat. Neurosci.* 2012, *15*, 477–486.

[6] Moeller, H. C., Mian, M. K., Shrivastava, S., Chung, B. G., Khademhosseini, A., *Biomaterials* 2008, *29*, 752–763.

[7] Hwang, Y. S., Chung, B. G., Ortmann, D., Hattori, N., Moeller, H. C., Khademhosseini, A., *Proc. Natl. Acad. Sci. USA* 2009, *106*, 16978–16983.

[8] Azarin, S. M., Lian, X., Larson, E. A., Popelka, H. M., de Pablo, J. J., Palecek, S. P., *Biomaterials* 2012, *33*, 2041–2049.

[9] Choi, Y. Y., Chung, B. G., Lee, D. H., Khademhosseini, A., Kim, J. H., Lee, S. H., *Biomaterials* 2010, *31*, 4296–4303.

[10] Chung, B. G., Choo, J., *Electrophoresis* 2010, *31*, 3014–3027.

[11] Chung, B. G., Lee, K. H., Khademhosseini, A., Lee, S. H., *Lab Chip.* 2012, *12*, 45–59.

[12] Whitesides, G. M., *Nature* 2006, *442*, 368–373.

[13] Weibel, D. B., Whitesides, G. M., *Curr. Opin. Chem. Biol.* 2006, *10*, 584–591.

[14] Keenan, T. M., Folch, A., *Lab Chip.* 2008, *8*, 34–57.

[15] Hung, P. J., Lee, P. J., Sabounchi, P., Lin, R., Lee, L. P., *Biotechnol. Bioeng.* 2005, *89*, 1–8.

[16] Di Carlo, D., Wu, L. Y., Lee, L. P., *Lab Chip.* 2006, *6*, 1445–1449.

[17] Hong, S., Pan, Q., Lee, L. P., *Integr. Biol.* 2012, *4*, 374–380.

[18] Torisawa, Y. S., Chueh, B. H., Huh, D., Ramamurthy, P., Roth, T. M., Barald, K. F., Takayama, S., *Lab Chip.* 2007, *7*, 770–776.

[19] Shin, H. S., Kim, H. J., Min, S. K., Kim, S. H., Lee, B. M., Jeon, N. L., *Biotechnol. Lett.* 2010, *32*, 1063–1070.

[20] Toh, Y. C., Voldman, J., *FASEB J.* 2011, *25*, 1208–1217.

[21] Blagovic, K., Kim, L. Y., Voldman, J., *PLoS One* 2011, *6*, e22892.

[22] Lee, J. M., Kim, J. E., Kang, E., Lee, S. H., Chung, B. G., *Electrophoresis* 2011, *32*, 3133–3137.

[23] Brian J. Kirby. *Micro- and Nanoscale Fluid Mechanics: Transport in Microfluidic Devices*, Cambridge University Press, 2010, pp. 14–19.

[24] Kim, M. C., Isenberg, B. C., Sutin, J., Meller, A., Wong, J. Y., Klapperich, C. M., *Lab Chip.* 2011, *11*, 1089–1095.

[25] Lee, S. H., Lumelsky, N., Studer, L., Auerbach, J. M., McKay, R. D., *Nat. Biotechnol.* 2000, *18*, 675–679.

[26] Kim, C., Lee, K. S., Bang, J. H., Kim, Y. E., Kim, M. C., Oh, K. W., Lee, S. H., Kang, J. Y., *Lab Chip.* 2011, *11*, 874–882.

[27] Kang, E., Choi, Y. Y., Jun, Y., Chung, B. G., Lee, S. H., *Lab Chip*. 2010, *10*, 2651–2654.

